Orthogonal Coordinates and Hyperquantization Algorithm. The NH_3 and H_3O^+ Umbrella Inversion Levels†

M. Ragni,‡ A. Lombardi,‡ P. R. Pereira Barreto,§ and A. C. Peixoto Bitencourt*,⊥

Dipartimento di Chimica, Universitá di Perugia, 06123 Perugia, Italy, Laboratório Associado de Plasma (LAP), Instituto Nacional de Pesquisas Espaciais (INPE)/MCT, CP 515 São José dos Campos, São Paulo CEP 1224 7-9 70, Brazil, and Centro de Formação de Professores, Universidade Federal do Recôncavo da Bahia (UFRB), Brazil

Received: July 7, 2009; Revised Manuscript Received: August 3, 2009

In order to describe the umbrella inversion mode, which is characteristic of AB_3-type molecules, we have introduced an alternative hyperspherical coordinate set based on a parametrization of Radau−Smith orthogonal vectors and have considered constraints which allow us to enforce the C_{3v} symmetry. Structural properties and electronic energies at equilibrium and barrier configurations have been obtained at MP2 and CCSD(T) levels of theory. Energy profiles have been calculated using the CCSD(T) method with an aug-cc-pVQZ basis set. The NH_3 and H_3O^+ umbrella inversion levels are obtained by the hyperquantization algorithm for a one-dimensional calculation, using a specially defined hyperangle as the inversion coordinate. The results are compared with experimental and theoretical energy levels, in particular, with those obtained by calculations based on two-dimensional models. The emerging picture of the umbrella inversion based on this hyperangular coordinate compares favorably with respect to the usual valence-type description.

1. Introduction

Tetratomic molecules, such as NH_3 and H_3O^+ considered in this paper, exhibit a characteristic mode, the "umbrella inversion". Such a mode of the intramolecular motion can be viewed as one of the simplest mechanisms of a chirality changing process (this at least from a classical mechanics viewpoint, which permits one to distinguish among the hydrogen atoms, or even quantum mechanically if they were properly isotopically labeled). Indeed, the problem of the inversion of chirality in molecules is of fundamental importance in chemistry, primarily because of selectivity for different enantiomers of the interactions in biological systems.[1] In previous work, we have extensively investigated the case of chirality inversion due to torsion around the −OO− and −SS− bonds. As the prototypical example involving four atoms or groups bound as a sequential chain, H_2O_2 presents an out-of-plane configuration, and the torsion around the dihedral angle HOOH leads to an inversion of chirality.[2,3] For an extensive treatment of this topic, see refs 2−6 and references therein, where, in particular, advantages have been shown of an approach based on coordinate sets obtained by a hyperspherical parametrization of orthogonal Jacobi-type vectors. In a similar spirit, we approached here another possible connectivity of four atoms, namely, that corresponding to the ramified one, exemplified by the cases of NH_3 [7] and H_3O^+ [8] (AB_3-type molecules). Both systems show a similar pyramidal structure, where the atom A is bound to three B atoms. In this case, the inversion of chirality due to the spatial orientations of the bonds follows a different mechanism referred to as umbrella inversion.

In this work, we study the umbrella inversion motion in hyperspherical coordinates, obtained by a parametrization of Radau−Smith[9] orthogonal vectors. The hyperspherical parametrization permits an extremely convenient representation of the vibro-rotational modes of the NH_3 and H_3O^+ systems, leading to a very simple kinetic energy operator. Indeed, we show that the umbrella inversion motion can be studied to first order, varying only one hyperangle.[10−12] This particular angle, here introduced enforcing C_{3v} symmetry in the Radau−Smith vector parametrization, remarkably coincides with that recommended[12] as a collective coordinate for the four-body problem in the symmetrical (inertial) parametrization. This angle is also defined in such a way that the corresponding part of the kinetic energy operator has a convenient form which can be solved by the hyperquantization algorithm.[13−15] This algorithm was originally developed for scattering problems, and this is the first time that it is used to calculate vibrational levels of a molecule. The reasons that led us to choose this approach are essentially based on the inherent simplicity of implementation and, as it is also shown here, on its fast performance.

The umbrella inversion levels for the two tested systems are calculated introducing also the separation in symmetries of the wave functions,[16] obtaining significant simplifications and reductions of calculation time. The results are in agreement with data available in the literature, and a remarkable result is that our inversion energy levels, calculated by a one-dimensional model, compare favorably with those obtained by two- or full-dimensional calculations. As shown in cases such as H_2O_2 and H_2S_2,[17,18] this is encouraging for the study of intermolecular interactions where a feasible quantum mechanical investigation of collisional dynamics requires a reduction of the number of active degrees of freedom.

The paper is organized as follows. In section 2, the coordinates of the problem are defined, and the relative Hamiltonian is considered. In section 3, the hyperquantization algorithm is briefly described, while in section 4, results obtained for the two systems under analysis are presented. In section 5, a preliminary discussion of the two-dimensional problem and adiabatic eigenvalue curves are presented. Remarks and perspectives are presented in section

† Part of the "Vincenzo Aquilanti Festschrift".

* To whom correspondence should be addressed. E-mail: ana.bitencourt@gmail.com.

‡ Universitá di Perugia.

§ Instituto Nacional de Pesquisas Espaciais (INPE)/MCT.

⊥ Centro de Formação de Professores, Universidade Federal do Recôncavo da Bahia (UFRB), Brazil.

10.1021/jp906415m
Published on Web 09/16/2009

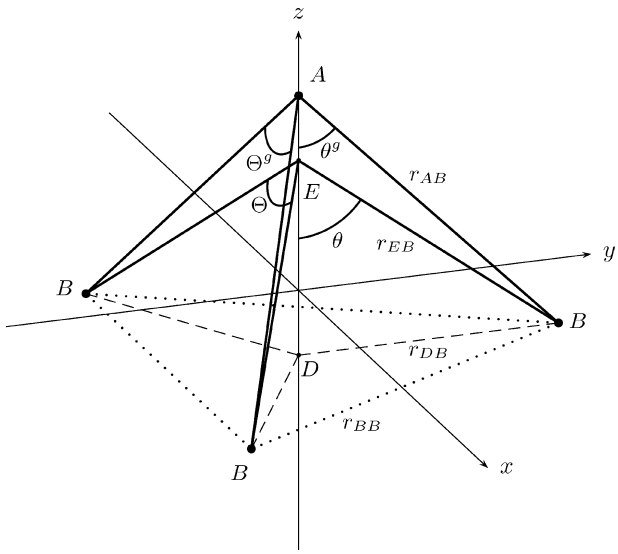

Figure 1. Geometry of an AB_3 system having C_{3v} symmetry. The z axis coincides with the C_3 symmetry axis. The particle A is taken as the heliocenter of the system. The three AB bond lengths (solid black lines) are equal and are denoted as r_{AB}. Due to the symmetry, the BB distances (dotted lines), denoted as r_{BB}, and the DB distances (dashed lines), denoted as r_{DB}, are also equal. The center of mass of the three B particles is denoted as D in the figure, while the center of mass of the whole system is at the origin of the Cartesian reference frame.

6. In Appendix A, some details can be found about the separation in symmetries of doubly symmetric matrices.

2. Coordinates and Hamiltonian for the AB_3 Umbrella Inversion Problem

Pyramidal molecules AB_3 exhibit a double minimum potential energy profile whose corresponding configurations preserve the C_{3v} symmetry. When the system crosses the barrier separating the two identical configurations, an inversion motion, commonly known as umbrella inversion, takes place. This suggests that a simple picture for a model of inversion, which is interesting because it involves also a change of chirality, can rely particularly on the hypothesis of symmetry conservation along the inversion path, where a single coordinate may be suitable to describe the process with sufficient accuracy. The optimal choice for such a coordinate is not obvious, especially if one aims at giving an approach to be valid in a number of cases.

The kinetic energy quantum operator in mass-scaled Radau−Smith vectors for four bodies,[10,11] after separation of the center of mass motion, is

$$\hat{T}(\mathbf{x}) = -\frac{\hbar^2}{2m}\left[\frac{\partial^2}{\partial(\mathbf{x}_1)^2} + \frac{\partial^2}{\partial(\mathbf{x}_2)^2} + \frac{\partial^2}{\partial(\mathbf{x}_3)^2}\right] \qquad (1)$$

where m is the total mass of the system and the vectors $\mathbf{x}_i$ (i = 1, 2, 3) represent the positions of the three particles B with respect to the canonical point E.[10,11] Figure 1 shows the Radau−Smith vectors for a pyramidal AB_3 molecular system, along with the position of points D and O (the center of the Cartesian reference frame) and the canonical point E of the vectors $\mathbf{x}_i$ (i = 1, 2, 3), whose position is found requiring that $r_{DE}^2 = r_{DO}r_{DA}$. The three equal angles $B\hat{A}B$ are denoted as Θ^g while the angles between the z axis and the AB bonds are denoted as θ^g. The superscript g stands for "geometrical" parametrization. The angles Θ and θ and the distances r_{EB} are related to the geometrical angles θ^g and Θ^g and to the modules of the vectors $\mathbf{x}_i$ and the hyperradius ρ, respectively, through the simple formulas in section 2.2.

The extreme simplicity of the operator of eq 1, due to the absence of coupling terms, contrasts with the form of analogous operators obtained using bond lengths, bond angles, and dihedral angles, where mixed second-order derivatives (see, for example, eq 9 in ref 7) lead to cumbersome expressions, making it difficult to develop efficient computational schemes. In fact, a simple modification of the geometrical coordinate set permits one to obtain diagonal kinetic energy operators, such as that of eq 1, preserving the physical meaning of the geometrical parameters.[10] Starting from eq 1, constraints can be applied in order to implement the hypothesis of symmetry conservation along the inversion path.

In spherical coordinates, $\mathbf{x}_i = (r_i,\vartheta_i,\varphi_i)$ (i = 1, 2, 3), and eq 1 becomes

$$\begin{aligned}\hat{T}(\mathbf{x}) &= -\frac{\hbar^2}{2m}\sum_{i=1}^{3}\left[\frac{1}{r_i^2}\frac{\partial}{\partial r_i}r_i^2\frac{\partial}{\partial r_i} + \frac{1}{r_i^2}\hat{Y}_i\right] \\ \hat{Y}_i &= \frac{1}{\sin\vartheta_i}\frac{\partial}{\partial\vartheta_i}\sin\vartheta_i\frac{\partial}{\partial\vartheta_i} + \frac{1}{\sin^2\vartheta_i}\frac{\partial^2}{\partial\varphi_i^2}\end{aligned} \qquad (2)$$

where $r_i = |\mathbf{x}_i| \geq 0$, $0 \leq \vartheta_i \leq \pi$, and $0 \leq \varphi_i < 2\pi$, i = 1, 2, 3.

2.1. Constraints. To ensure that the C_{3v} symmetry is conserved along the umbrella inversion path, some of the degrees of freedom must be constrained. The AB bond lengths (see Figure 1) have to be equal at each given instant of the inversion motion, only their symmetric stretching being allowed. To this aim, the following parametrization of the Radau−Smith vector lenghts, r_1,r_2,r_3, is adopted, in analogy with the approach of ref 11

$$\begin{aligned}r_1 &= \rho\cos\chi_2\cos\chi_1 \\ r_2 &= \rho\cos\chi_2\sin\chi_1 \\ r_3 &= \rho\sin\chi_2\end{aligned} \qquad (3)$$

where, to achieve a one-to-one representation of the C_{3v} symmetry molecular configurations in terms of the new coordinates, the ranges of variables must be $0 \leq \rho \leq \infty$ and $0 \leq \chi_1$, $\chi_2 \leq \pi/2$. The above coordinate transformation leads to the following kinetic energy operator

$$\hat{T}(\mathbf{x}) = -\frac{\hbar^2}{2m}\left[\rho^{-8}\frac{\partial}{\partial\rho}\rho^8\frac{\partial}{\partial\rho} + \rho^{-2}\Delta(\Omega)\right] \qquad (4)$$

$$\begin{aligned}\Delta(\Omega) = {} & \frac{1}{\cos^5(\chi_2)\sin^2(\chi_2)}\frac{\partial}{\partial\chi_2}\cos^5(\chi_2)\sin^2(\chi_2)\frac{\partial}{\partial\chi_2} + \\ & \frac{1}{\cos^2(\chi_2)\cos^2(\chi_1)\sin^2(\chi_1)}\frac{\partial}{\partial\chi_1}\cos^2(\chi_1)\sin^2(\chi_1)\frac{\partial}{\partial\chi_1} + \\ & \frac{1}{\cos^2(\chi_2)\cos^2(\chi_1)}\left[\frac{1}{\sin\vartheta_1}\frac{\partial}{\partial\vartheta_1}\sin\vartheta_1\frac{\partial}{\partial\vartheta_1} + \frac{1}{\sin^2\vartheta_1}\frac{\partial^2}{\partial\varphi_1^2}\right] + \\ & \frac{1}{\cos^2(\chi_2)\sin^2(\chi_1)}\left[\frac{1}{\sin\vartheta_2}\frac{\partial}{\partial\vartheta_2}\sin\vartheta_2\frac{\partial}{\partial\vartheta_2} + \frac{1}{\sin^2\vartheta_2}\frac{\partial^2}{\partial\varphi_2^2}\right] + \\ & \frac{1}{\sin^2(\chi_2)}\left[\frac{1}{\sin\vartheta_3}\frac{\partial}{\partial\vartheta_3}\sin\vartheta_3\frac{\partial}{\partial\vartheta_3} + \frac{1}{\sin^2\vartheta_3}\frac{\partial^2}{\partial\varphi_3^2}\right]\end{aligned} \qquad (5)$$

where $\Delta(\Omega)$ is the so-called grand angular operator and Ω collectively denotes all angles. It can be verified from eq 3 that

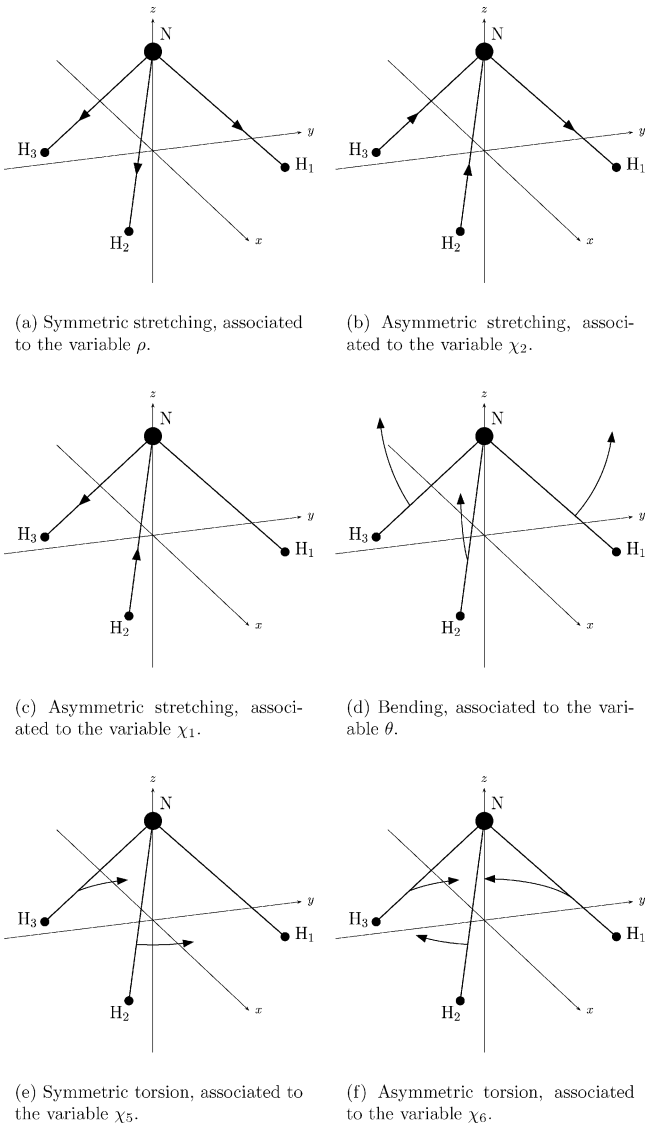

(a) Symmetric stretching, associated to the variable ρ.

(b) Asymmetric stretching, associated to the variable χ_2.

(c) Asymmetric stretching, associated to the variable χ_1.

(d) Bending, associated to the variable θ.

(e) Symmetric torsion, associated to the variable χ_5.

(f) Asymmetric torsion, associated to the variable χ_6.

Figure 2. The normal modes of the AB_3 system are schematically illustrated, and the correspondences with the coordinates developed in this work are assigned. The coordinate θ correctly describes the umbrella inversion motion, as illustrated in (d).

the symmetric stretching condition $r_1 = r_2 = r_3$ is obtained for $\chi_1 = 45°$ and $\tan(\chi_2) = \sin(\chi_1)$. Therefore, the modes of stretching are forced to be symmetric by constraining the χ_1 and χ_2 coordinates to the above fixed values (see below, section 2.2 and Figure 2 for the assignment of the correspondence between normal modes and the hyperspherical coordinates introduced here). Also, the C_{3v} symmetry is retained only if the angles φ_1, φ_2, and φ_3 are fixed and each one differs from the other two by $\pi/3$ (for example $\varphi_1 = 0$, $\varphi_2 = \pi/3$, and $\varphi_3 = 2\pi/3$).

Applying the above constraints, the grand angular operator simplifies as follows

$$\Delta(\Omega) = 3\sum_{i=1}^{3} \frac{1}{\sin\vartheta_i}\frac{\partial}{\partial\vartheta_i}\sin\vartheta_i\frac{\partial}{\partial\vartheta_i} \tag{6}$$

A further constraint must be applied to the three angles ϑ_i, which must be equal during the inversion motion ($\vartheta_1 = \vartheta_2 = \vartheta_3$). This condition is achieved by a new parametrization of $\vartheta_1,\vartheta_2,\vartheta_3$ as a function of a new coordinate θ and two variables χ_3 and χ_4 (see ref 12 for a discussion about the θ angle)

$$\begin{aligned}\vartheta_1 &= \sqrt{3}\theta\cos(\chi_4)\cos(\chi_3)\\ \vartheta_2 &= \sqrt{3}\theta\cos(\chi_4)\sin(\chi_3)\\ \vartheta_3 &= \sqrt{3}\theta\sin(\chi_4)\end{aligned} \tag{7}$$

Inverting the above formulas, it can be seen that

$$\theta = \sqrt{\frac{\vartheta_1^2 + \vartheta_2^2 + \vartheta_3^2}{3}} \qquad 0 \le \theta \le \pi \tag{8}$$

where the $\sqrt{3}$ factor scales the upper limit of θ to π, as required by the range of Legendre polynomials, which will be used as the basis set for solving the corresponding one-dimensional eigenvalue problem (see section 2.3). For χ_3 and χ_4, one has that

$$\begin{aligned}\chi_3 &= \arctan\frac{\vartheta_2}{\vartheta_1} \quad 0 \le \chi_3 \le \pi/2\\ \chi_4 &= \arcsin\frac{\vartheta_3}{\theta\sqrt{3}} \quad 0 \le \chi_4 \le \pi/2\end{aligned} \tag{9}$$

The partial derivatives with respect to θ_1, θ_2, and θ_3 appearing in the grand angular operator of eq 6 can be obtained in terms of the new coordinates θ, χ_3, and χ_4 by differentiation of the formulas given by eqs 8 and 9

$$\begin{aligned}\frac{\partial}{\partial\vartheta_1} &= \frac{\cos\chi_3\cos\chi_4}{\sqrt{3}}\frac{\partial}{\partial\theta} - \frac{\sin\chi_3}{\sqrt{3}\theta\cos\chi_4}\frac{\partial}{\partial\chi_3} - \frac{\cos\chi_3\sin\chi_4}{\sqrt{3}\theta}\frac{\partial}{\partial\chi_4}\\ \frac{\partial}{\partial\vartheta_2} &= \frac{\sin\chi_3\cos\chi_4}{\sqrt{3}}\frac{\partial}{\partial\theta} + \frac{\cos\chi_3}{\sqrt{3}\theta\cos\chi_4}\frac{\partial}{\partial\chi_3} - \frac{\sin\chi_3\sin\chi_4}{\sqrt{3}\theta}\frac{\partial}{\partial\chi_4}\\ \frac{\partial}{\partial\vartheta_3} &= \frac{\sin\chi_4}{\sqrt{3}}\frac{\partial}{\partial\theta} + \frac{\cos\chi_4}{\sqrt{3}\theta}\frac{\partial}{\partial\chi_4}\end{aligned} \tag{10}$$

From the condition

$$\theta = \vartheta_1 = \vartheta_2 = \vartheta_3 \tag{11}$$

it follows that χ_3 and χ_4 are equal to $\pi/4$ and $\arcsin(1/\sqrt{3})$, respectively. The angle θ has interesting properties, which have been described in ref 12, where an identical coordinate was considered. Specifically, this angle was related there to the largest of three principal moments of inertia or to the two largest ones in the case of an oblate top molecule (e.g., ammonia).

2.2. Details on the Coordinate Set. Low-amplitude variations of the hyperspherical coordinates considered here can be put into relationship with the normal-mode vibrations of AB_3 molecular systems. It can be seen from eq 3 that ρ is related to the symmetric stretching of the system (Figure 2a), while the two angles χ_2 and χ_1 correspond to the two asymmetric stretching modes (Figure 2b and c). As illustrated above, θ (see eq 8) correlates with the bending mode that leads to the umbrella inversion (Figure 2d).

Let us perform another coordinate transformation on the angles φ_1, φ_2, and φ_3 of eq 2, introducing the coordinates ϕ, χ_6, and χ_5 so that

$$\begin{aligned} \varphi_1 &= \phi \cos\chi_6 \cos\chi_5 \\ \varphi_2 &= \phi \cos\chi_6 \sin\chi_5 \\ \varphi_3 &= \phi \sin\chi_6 \end{aligned} \tag{12}$$

In this way, the variables χ_5 and χ_6 correlate with the symmetric and asymmetric torsion around the z axis (Figure 2e and f). The variable ϕ is related to the ordinary external rotation, as well as χ_3 and χ_4, eq 9.

Referring to Figure 1 and under the constraints given in section 2.1, the canonical point E of the Radau−Smith vectors is calculated from the following equations

$$\begin{aligned} r_{AD} &= r_{AB}\cos(\theta^g) \\ r_{DO} &= \frac{m_A}{m} r_{AD} \\ r_{DE} &= \sqrt{\frac{m_A}{m}} r_{AD} \end{aligned} \tag{13}$$

where m_A is the mass of the particle A and m is the total mass of the system (the superscript g in θ^g stands for geometrical; indeed, this is the geometrical parameter strictly related to our coordinate θ; see below). These equations are used to obtain the expressions of the length r_{EB} of the Radau−Smith vectors and of the angle θ, as a function of θ^g and r_{AB}

$$\begin{aligned} r_{EB} &= r_{AB}\left(1 - \frac{3m_B}{m}\cos^2(\theta^g)\right)^{1/2} \\ \cos(\theta) &= \left(\frac{m_A \cos^2(\theta^g)}{m - 3m_B\cos^2(\theta^g)}\right)^{1/2} \end{aligned} \tag{14}$$

where m_B is the mass of the particles B. Other useful relationships are

$$\begin{aligned} r_{BB} &= \sqrt{3} r_{AB}\sin(\theta^g) \\ \cos(\Theta^g) &= 1 - \frac{3}{2}\sin^2(\theta^g) \\ \cos(\Theta) &= 1 - \frac{3}{2}\frac{1}{1 + \frac{m_A}{m}\cot^2(\theta^g)} \end{aligned} \tag{15}$$

From the above equations, it is also found that (see eq 16 of ref 12)

$$\sin^2(\theta) = \frac{4\sin^2(\Theta^g/2)}{3\frac{m_A}{m} + 12\frac{m_B}{m}\sin^2(\Theta^g/2)} \tag{16}$$

The lenghts of the vectors $\mathbf{x}_i$, (i = 1, 2, 3; see eq 1) and the hyperradius ρ are connected to the distances r_{EB} through the following formulas

$$\begin{aligned} |\mathbf{x}_l| &= \sqrt{\frac{m_B}{m}} r_{EB} \\ \rho &= \sqrt{\frac{3m_B}{m}} r_{EB} \end{aligned} \tag{17}$$

Knowing the hyperradius ρ and the angle θ, it is possible to calculate the moments of inertia of the AB_3 system with respect to the three reference axes of Figure 1

$$\begin{aligned} I_z &= m\rho^2 \sin^2\theta \\ I_x &= I_y = m\rho^2\left(\cos^2\theta + \frac{1}{2}\sin^2\theta\right) \end{aligned} \tag{18}$$

so that the total inertia is simply[12]

$$I = I_x + I_y + I_z = 2m\rho^2 \tag{19}$$

2.3. Solutions at Fixed ρ. A treatment similar to that described in section 2.2 can be applied to the three angles φ_1, φ_2, and φ_3 of eq 2.

In conclusion, the problem is reduced to a two-dimensional one, whose corresponding Hamiltonian operator is

$$\hat{H}(\rho,\theta) = \hat{T}(\rho,\theta) + V(\rho,\theta) \tag{20}$$

where the kinetic part $\hat{T}(\mathbf{x})$ is

$$\begin{aligned} \hat{T}(\rho,\theta) &= -\frac{\hbar^2}{2m}\left[\rho^{-8}\frac{\partial}{\partial\rho}\rho^8\frac{\partial}{\partial\rho} + \frac{1}{\rho^2}\Delta(\theta)\right] \\ \Delta(\theta) &= \frac{1}{\sin\theta}\frac{\partial}{\partial\theta}\sin\theta\frac{\partial}{\partial\theta} \end{aligned} \tag{21}$$

The solutions of the angular part of the kinetic energy operator, $\Delta(\theta)$ (eq 21), are the Legendre polynomials $P_l(\theta)$ in $\cos(\theta)$ (l = 0, 1, 2, ...)

$$\begin{aligned} \mathrm{P}_l(\theta) &= \sqrt{l + \frac{1}{2}}\frac{1}{2^l l!}\frac{\mathrm{d}^l}{\mathrm{d}(\cos\theta)^l}(\cos^2\theta - 1)^l \\ \Delta(\theta)\mathrm{P}_l(\theta) &= -l(l+1)P_l(\theta) \end{aligned} \tag{22}$$

that obey the orthogonality relationship

$$-\int_0^\pi P_l^*(\theta)P_{l'}(\theta)\mathrm{d}\cos(\theta) = \delta_{l,l'} \tag{23}$$

These wave functions are a convenient basis set for the expansion of the solutions of eq 21 at a fixed value of ρ.

3. Hyperquantization Algorithm

To solve the angular part of eq 20, we use the so-called hyperquantization algorithm (for a complete account, see refs 13−15). Let us give now some details about the underlying theory and the method.

Hyperquantization is essentially a discretization technique aimed at solving eigenvalue equations typical of chemical problems. Therefore, as a first step, one has to introduce the

discrete analogues of the Legendre polynomials $P_l(\theta)$. Let us define the discrete variable ξ so that

$$-\cos(\theta) = \frac{2\xi}{M} = x \tag{24}$$

where $\xi = -M/2, -M/2 + 1, ..., M/2 - 1, M/2$ and M is the number of discretization intervals. For our purposes, it is convenient to scale the polynomials $P_l(\theta)$ by a normalization factor, denoted as K_l, so that

$$\begin{aligned} P_l^M(\xi) &= K_l \frac{\mathrm{d}^l}{\mathrm{d}x^l}(x^2 - 1)^l \\ \sum_{l=0}^{M} P_l^M(\xi) P_l^M(\xi') &= \delta_{\xi'-\xi} \end{aligned} \tag{25}$$

The last equation above is strictly valid in the case that $M \rightarrow \infty$.

With this procedure, the $P_l(\xi)$ function can be considered to be discretized with respect not only to the degree l but also to the variable ξ. The idea at the basis of the hyperquantization algorithm consists of an inversion of roles between l and ξ, treating l as an integration variable and ξ and ξ' as labels of the elements of the matrix **H** representing the Hamiltonian operator $\hat{H}$ (see eqs 19 and 20) in the discrete polynomials basis. For a given value of the hyperradius ρ, an element $H_\rho^{\xi',\xi}$ of the matrix **H** is

$$\begin{aligned} H_\rho^{\xi',\xi} &= \sum_{l=0}^{\infty} P_l^M(\xi') \left[-\frac{\hbar^2}{2m\rho^2} \Delta^M(\xi) + V^M(\rho, \xi) \right] P_l^M(\xi) \\ &= \frac{\hbar^2}{2m\rho^2} \sum_{l=0}^{\infty} [l(l+1) P_l^M(\xi') P_l^M(\xi)] + V^M(\rho, \xi) \delta_{\xi',\xi} \end{aligned} \tag{26}$$

The $M + 1$ eigenvalues $\varepsilon_{\rho,j}$ of the matrix **H** are labeled by integer numbers j. The corresponding eigenvectors $C_{\rho,j}(\xi)$ are the coefficients of the expansion of the wave function $\psi_{\rho,j,l}$ in the polynomials basis set

$$\psi_{\rho,j,l} = \sum_{\xi=0}^{M} C_{\rho,j}(\xi) P_l^M(\xi) \tag{27}$$

and it can be seen that

$$\psi_{\rho,j}(\xi') = \sum_{l=0}^{\infty} P_l^M(\xi') \sum_{\xi=0}^{M} C_{\rho,j}(\xi) P_l^M(\xi) = C_{\rho,j}(\xi') \tag{28}$$

In other words, the eigenvectors are directly the wave functions for which we are looking for.

The matrix elements given by eq 26 can be calculated numerically or by the following recurrence relation

$$a(\xi) P_l^M(\xi - 1) + (b(\xi) - l(l+1)) P_l^M(\xi) + c(\xi) P_l^M(\xi + 1) = R(l, \xi, M) \tag{29}$$

where $R(l,\xi,M)$ is a residual term for which

$$\lim_{M \rightarrow \infty} R(l, \xi, M) = 0 \tag{30}$$

If M is large enough, the residual functions $R(l,\xi,M)$ approximately satisfies the above condition, and the coefficients a, b, and c can be calculated with sufficient accuracy. Since $P_0^M(\xi) = k(l)$, it holds that $a(\xi) + b(\xi) + c(\xi) = 0$. Setting $l = 1$, by properly handling the formulas, one has that

$$a(\xi)(-\xi + 1) - (b(\xi) - 2)(\xi) + c(\xi)(-\xi - 1) = 0 \tag{31}$$

It follows that

$$\begin{aligned} a(\xi) - c(\xi) &= -2\xi \\ a(\xi) &= -\frac{b(\xi)}{2} - \xi \\ c(\xi) &= -\frac{b(\xi)}{2} + \xi \end{aligned} \tag{32}$$

Starting from these results, for $l = 2$, one obtains

$$\begin{aligned} a(\xi) &= \xi^2 - \xi - \frac{M^2}{4} \\ b(\xi) &= -2\xi^2 + \frac{M^2}{2} \\ c(\xi) &= \xi^2 + \xi - \frac{M^2}{4} \end{aligned} \tag{33}$$

while for $l = 3$

$$\begin{aligned} a(\xi) &= \xi^2 - \xi - \frac{M^2}{4} - \frac{1}{3} \\ b(\xi) &= -2\xi^2 + \frac{M^2}{2} + \frac{2}{3} \\ c(\xi) &= \xi^2 + \xi - \frac{M^2}{4} - \frac{1}{3} \end{aligned} \tag{34}$$

The dependence of the coefficients from the grid size M changes for different values of l, and the preferred form is the one ensuring faster converge.

An efficient method to determine the above coefficients has been developed by Aquilanti et al.[13−15] by representing the Legendre polynomials in terms of $3j$ symbols and exploiting some well-known properties of these. The recurrence relation satisfied by $3j$ symbols permits to approximate the coefficients with a residual term $R(l,\xi,M)$ that tends to zero more rapidly as M increases. These approximate expressions are as follows

$$\begin{aligned} a(\xi) &= \xi^2 - \xi - \frac{M^2}{4} - \frac{M}{2} \\ b(\xi) &= -2\xi^2 + \frac{M^2}{2} + M \\ c(\xi) &= \xi^2 + \xi - \frac{M^2}{4} - \frac{M}{2} \end{aligned} \tag{35}$$

TABLE 1: $R(l,\xi,M)$ Expressions Obtained by Equation 29 Using the Coefficients Given in Equations 33 (Second Column), 34 (Third Column), and 35 (Fourth Column)[a]

l	$l = 0, 1, 2$	$l = 0, 1, 3$	refs 13−15
0	0	0	0
1	0	0	0
2	0	$-4/M^2$	$-6/M$
3	$-40\xi/M^3$	0	$(60\xi/M^2) - (40\xi/M^3)$
4	$(700\xi^2/M^4) - (35/M^2)$	$-(25/M^2) + (420\xi^2/M^4) - (140/3M^4)$	$(15/M) - (35/M^2) - (420\xi^2/M^3) - (70/M^3) + (700\xi^2/M^4)$
5	$(770\xi/M^3) - (7560\xi^3/M^5) - (504\xi/M^5)$	$(630\xi/M^3) - (5880\xi^3/M^5) + (336\xi/M^5)$	$-(210\xi/M^2) + (770\xi/M^3) + (2520\xi^3/M^4) + (1260\xi/M^4) - (7560\xi^3/M^5) - (504\xi/M^5)$

[a] These expressions must be multiplied by the normalization factor K_l.

TABLE 2: Basis Set Dependence Study for the Gometries of NH_3 and H_3O^+ Systems at a CCSD(T) Level of Theory[a]

NH_3						
basis set	r_{NH}(eq) [Å]	r_{NH}(bar) [Å]	Θ_{eq} [deg]	E_{eq} [hartree]	E_{bar} [hartree]	bar [cm^{-1}]
cc-pVDZ	1.0273	1.0052	114.8749	−56.4162550	−56.3886572	6057.321
aug-cc-pVDZ	1.0237	1.0054	112.8306	−56.4255199	−56.4162550	2033.513
cc-pVTZ	1.0141	0.9952	113.0816	−56.4731973	−56.4630008	2237.985
aug-cc-pVTZ	1.0149	0.9975	112.4036	−56.4805626	−56.4717392	1936.610
cc-pVQZ	1.0125	0.9949	112.6053	−56.4930532	−56.4838236	2025.765
aug-cc-pVQZ	1.0128	0.9959	112.2686	−56.4957326	−56.4872261	1867.055
cc-pV5Z	1.0121	0.9952	112.2821	−56.4994511	−56.4908220	1893.964
aug-cc-pV5Z	1.0123	0.9956	112.2549	−56.5002838	−56.4918659	1847.608
references	1.0124[26]		112.15[26]			1833.9[21] 1845.6 ± 46.8[27] 1792[28]
H_3O^+						
basis set	R_{eq} [Å]	R_{bar} [Å]	Θ_{eq} [deg]	E_{eq} [hartree]	E_{bar} [hartree]	bar [cm^{-1}]
cc-pVDZ	0.9841	0.9762	109.5335	−76.5295323	−76.5241240	1187.044
aug-cc-pVDZ	0.9831	0.9755	107.9362	−76.5451975	−76.5414621	819.867
cc-pVTZ	0.9779	0.9701	107.3881	−76.6114941	−76.6080530	755.272
aug-cc-pVTZ	0.9792	0.9712	107.3900	−76.6156547	−76.6119957	803.098
cc-pVQZ	0.9760	0.9687	107.0655	−76.6355589	−76.6323718	699.523
aug-cc-pVQZ	0.9765	0.9691	107.1048	−76.6370193	−76.6338008	706.415
cc-pV5Z	0.9759	0.9686	107.0253	−76.6430749	−76.6399662	682.315
aug-cc-pV5Z	0.9761	0.9687	107.0191	−76.6436592	−76.6405475	682.973
references	0.9744[29]		113.58[29]			650[28]

[a] The values of the geometrical parameters are given for the equilibrium (eq) and barrier (bar) configurations.

They are similar to those reported in eq 33, with similar residual functions $R(l,\xi,M)$, as shown in Table 1.

There are two remarkable aspects involving the potential and kinetic parts of the Hamiltonian. Equation 26 implies that no integral on the potential part has to be calculated numerically, a considerable advantage in terms of computation time. Moreover, the potential energy matrix is diagonal, with elements equal to the values of the potential calculated at angles $\arccos(-2\xi/M)$. Also, due to the three-term recurrence relation of eq 29, the kinetic energy operator matrix has a tridiagonal form. As a consequence, the matrix **H** is also tridiagonal, with elements $H_\rho^{\xi',\xi}$, which are as follows

$$\begin{aligned} H_\rho^{\xi',\xi} &= \frac{\hbar^2}{2m\rho^2}\sum_l^\infty P_l^M(\xi')[a(\xi)P_l^M(\xi-1) + b(\xi)P_l^M(\xi) + \\ &\qquad c(\xi)P_l^M(\xi+1)] + V(\xi')\delta_{\xi',\xi} \\ &= \frac{\hbar^2}{2m\rho^2}[a(\xi)\delta_{\xi',\xi-1} + b(\xi)\delta_{\xi',\xi} + c(\xi)\delta_{\xi',\xi+1}] + V(\xi')\delta_{\xi,\xi'} \end{aligned} \tag{36}$$

For the specific molecules of interest here, such as NH_3 and H_3O^+, the potential energy surface is symmetric with respect to $\theta = \pi/2$, and the **H** matrix turns out to be doubly symmetric (see Appendix A and ref 16 for details). Note that doubly symmetric matrices can be partitioned into two submatrices by a similarity transformation in such a way that the diagonalization of **H** greatly simplifies. For the even simpler case of a tridiagonal form, the transformation, for example of a 5 × 5 matrix, is explicitly as follows

$$\begin{pmatrix} a & d & 0 & 0 & 0 \\ d & b & e & 0 & 0 \\ 0 & e & c & e & 0 \\ 0 & 0 & e & b & d \\ 0 & 0 & 0 & d & a \end{pmatrix} \Rightarrow \begin{pmatrix} a & d & 0 & 0 & 0 \\ d & b & e\sqrt{2} & 0 & 0 \\ 0 & e\sqrt{2} & c & 0 & 0 \\ 0 & 0 & 0 & b & d \\ 0 & 0 & 0 & d & a \end{pmatrix} \tag{37}$$

and leads to separation in 3 × 3 and 2 × 2 blocks.

4. The NH_3 and H_3O^+ Systems

In Table 2, we report results of a basis set study dependence for the geometrical parameters of NH_3 and H_3O^+ systems, for both the equilibrium and barrier (D_{3h} planar) configurations. Bond lengths, angles, and energies are calculated at a CCSD(T) level. All calculations have been carried out with the Gaussian

TABLE 3: Geometry Parameters, Energies, and Normal-Mode Frequencies (MP2 Level) for the Equilibrium and Barrier Configurations of NH_3, from MP2 and CCSD(T) Level Calculations[a]

MP2/aug-cc-pVQZ			
geometry	equilibrium	barrier	barrier height (cm^{-1})
r_{NH} (Å)	1.008 (1.0124)[26]	0.993	
θ^g (degrees)	68.240 (67.85)[26]	90.000	
energy (uu)	−56.50818360	−56.50062321	1659.314

normal modes (cm^{-1})	equilibrium	barrier	associated coordinate
A1, A2″	1028.67 (1022)[26]	−826.46	θ
2E, 2E′	1673.19 (1691)[26]	1585.69	χ_5,χ_6
A1, A1′	3527.02 (3506)[26]	3664.49	ρ
2E, 2E′	3676.50 (3577)[26]	3889.68	χ_1,χ_2

CCSD(T)/aug-cc-pVQZ Level			
geometry	equilibrium	barrier	barrier height (cm^{-1})
r_{NH} (Å)	1.013 (1.0124)[26]	0.996	
θ^g (degrees)	67.733 (67.85)[26]	90.000	
r_{EH} (Å)	1.000	0.996	
θ (degrees)	69.629	90.000	
energy (ua)	−56.4957326	−56.4872261	1866.961 (1845.6 ± 46.8)[27]

[a] Values from the literature are in brackets. The assignment of normal modes of vibrations to our coordinates (see section 2.2) is reported.

package.[19] The data show that the energy decreases as the number of basis functions increases. In Table 3, we list geometrical parameters and electronic energies for the NH_3 molecule at the equilibrium and barrier configurations, calculated with an aug-cc-pVQZ basis set at MP2 and CCSD(T) levels of theory. For the MP2 level, the normal modes of vibration and the values of the hyperradius ρ and of the angle θ are also given. Note that the hyperradius ρ is directly connected to the distances r_{EB} and r_{AB} (the NH distance for the NH_3 molecule) through the formulas given in eq 17.

Comparing the values of the geometrical parameters at the equilibrium and barrier configurations, it can be seen that, moving along the umbrella inversion path, the r_{NH} bond lengths vary slightly; therefore, one expects only small variations for the hyperradius ρ, which therefore behaves approximately as a separable variable with respect to θ. As usual in the case of quantum reactive scattering, the hyperradial and hyperangular part of eqs 20 and 21 can well be treated separately.

We have used the CCSD(T) method and an aug-cc-pVQZ basis set to calculate the full inversion energy profiles of these molecules. This choice is justified also on the basis of previous studies.[7,8] Figure 3 compares the minimum-energy path for the inversion of NH_3 and the corresponding potential profile obtained by solving the one-dimensional problem fixing ρ at the equilibrium value. A profile obtained by fixing r_{NH} to its value at the equilibrium is also shown.

In Table 4, we report geometrical parameters for the H_3O^+ molecule at the equilibrium and barrier configurations. As for the case of NH_3, the hyperradius ρ is approximatively constant, and this again justifies the separation of variables ρ and θ in the solution of the corresponding eq 21.

The second step has been the calculation of the inversion vibrational energy levels. The umbrella inversion energy levels have been obtained by solving a one-dimensional eigenvalue problem (see eqs 20 and 21) by the hyperquantization algorithm

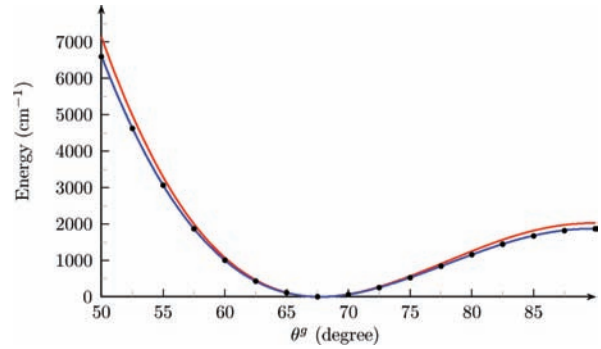

Figure 3. Potential energy profiles as a function of the θ^g angle for the NH_3 system. Dots represent the energy values optimized with respect to the hyperradius ρ. The blue curve is obtained fixing ρ at its equilibrium value. The red curve is obtained fixing r_{NH} at its equilibrium value.

TABLE 4: As in Table 3 for the H_3O^+ Molecule

ump2=full/aug-cc-pvqzc			
geometry	equilibrium	barrier	barrier height (cm^{-1})
r_{OH} (Å)	0.976 (0.9744)[29]	0.969	
θ^g (degrees)	72.900 (66.42)[29]	90.000	
energy (ua)	−76.65462689	−76.65165810	651.574

normal modes (cm^{-1})	equilibrium	barrier	associated coordinate
A1, A2″	886.30 (1050)[26]	−658.43	θ
2E, 2E′	1693.03 (1550)[26]	1627.04	χ_5,χ_6
A1, A1′	3595.95 (3760)[26]	3649.97	ρ
2E, 2E′	3704.59 (3870)[26]	3808.18	χ_1,χ_2

CCSD(T)/aug-cc-pvqz Level			
geometry	equilibrium	barrier	barrier height (cm^{-1})
r_{OH} (Å)	0.976 (0.9744)[29]	0.969	
θ^g (degrees)	72.872 (66.42)[29]	90.000	
r_{EH} (Å)	0.970	0.969	
θ (degrees)	74.219	90.000	
energy (ua)	−76.6370193	−76.6338007	706.401(650)[28]

(see section 3). As pointed out in previous sections, the corresponding one-dimensional Hamiltonian involves the θ coordinate and has a simple form (eq 21) that makes it particularly convenient to apply the hyperquantization.[13−15] The doubly symmetric character (see at the end of section 3) and the tridiagonal form of the matrix **H** to be diagonalized permits a significant reduction of calculation time. The symmetric and antisymmetric character of the eigenfunctions of two split levels has been taken into account. It helps when the energy splitting is small, as in the case of NH_3, where the two lowest energy levels are nearly degenerate but belong to states of different symmetry. It can be of help also in adiabatic (with respect to the hyperradius ρ) eigenvalue curve calculation, when, for a given value of ρ, different eigenfunctions may have nearly degenerate eigenvalues. According to the notation in the literature, in the following, the symmetric and antisymmetric levels will be indicated, respectively, by $n\nu_2^+$ and $n\nu_2^-$, where n numbers the levels. The two lowest levels ($n = 0$) are indicated with GS^+ (symmetric ground state) and GS^- (antisymmetric ground state).

From test calculations, we verified that a sufficiently large grid for the hyperquantization algorithm for the condition of eq 30 to be fulfilled should contain at least 3601 points (3600

TABLE 5: Umbrella Inversion Energy Levels of NH_3 for Three Different Fixed Values of the Hyperradius ρ[a]

	ρ^{e} [b]	ρ^{m} [c]	ρ^{b} [d]	surface[7]	theory[7]	exptl.[21]
GS^+	0.000	0.000	0.000	0.000	0.00	0.00
GS^-	1.257	1.309	1.361	1.258	0.96	0.793
ν_2^+	904.523	903.543	902.607	904.504	922.92	932.43
ν_2^-	956.521	957.170	957.883	956.527	964.74	968.12
$2\nu_2^+$	1545.695	1544.346	1543.153	1545.693	1577.97	1598.47
$2\nu_2^-$	1877.746	1880.517	1883.393	1877.792	1882.32	1882.18
$3\nu_2^+$	2388.918	2393.256	2397.751	2388.998	2387.96	2384.17
$3\nu_2^-$	2925.279	2932.099	2939.049	2925.404	2909.76	2895.61
$4\nu_2^+$	3512.634	3521.687	3530.906	3512.787	3485.55	
$4\nu_2^-$	4136.877	4148.248	4159.781	4137.072	4093.93	

[a] The energies have been obtained using inversion potential energy profiles calculated at the CCSD(T)/aug-cc-pVQZ level and minimized with respect to all of the other degrees of freedom. A hyperquantization grid of 3601 interpolated points has been used. Theoretical and experimental values for comparison are also reported in the last two columns. The fifth column reports the energy levels calculated using the potential energy surface developed in ref 7, freezing ρ at its equilibrium value. The values are taken with respect to the zero-point energy, which is 506.530, 506.574, and 506.863 cm^{-1} for ρ frozen at equilibrium, the middle point, and the barrier value respectively, and 506.463 cm^{-1} for values obtained from the surface of ref 7. [b] ρ frozen at the equilibrium value. [c] ρ frozen at the middle point value. [d] ρ frozen at the barrier value.

TABLE 6: Umbrella Inversion Energy Levels for the H_3O^+ System[a]

	surface[8]	theory[8]	exptl.[23−25]
GS^+	0.000	0.00	0.000
GS^-	59.196	52.29	55.3484
ν_2^+	584.979	588.31	581.18
ν_2^-	972.321	959.75	954.40
$2\nu_2^+$	1502.023	1482.12	1475.44
$2\nu_2^-$	2086.903	2056.61	
$3\nu_2^+$	2724.585	2683.15	
$3\nu_2^-$	3406.702	3352.54	
$4\nu_2^+$	4127.287		
$4\nu_2^-$	4882.156		

[a] The energy is minimized with respect to all of the other degrees of freedom. The second column reports the results obtained using a grid of 3601 points for the hyperquantization algorithm and the potential energy surface of ref 8. The zero-point energy is 372.772 cm^{-1}. Theoretical and experimental data are reported for comparison.

intervals) to guarantee accurate results such as those presented in Tables 5 and 6. Unfortunately, the ab initio calculation of the grid points to be used in the hyperquantization is very computer-demanding. To circumvent this problem, we calculated a reduced number of ab initio grid points and obtained additional points by a four-point Lagrange interpolation (see ref 20). Figure 4 shows the Lagrange interpolation function of 181 ρ-fixed ab initio points. From the interpolation functions, we obtained 3601 grid points used to build up the grid for the hyperquantization algorithm, avoiding long calculations of ab initio points that would not improve the accuracy of the energy levels.

4.1. NH_3 Potential and Umbrella Inversion Levels. The angle between the NH bonds and the C_3 molecular symmetry axis is denoted as θ^g in Figure 1. This geometrical parameter has been used to calculate the inversion potential energy profile from which the vibrational energy levels corresponding to the inversion motion have been obtained. Equation 14 gives the coordinate transformation that connects θ^g to the hyperangle θ, leading, as pointed out in section 2.2, to an extremely simple one-dimensional Hamiltonian operator (eq 21) that has been

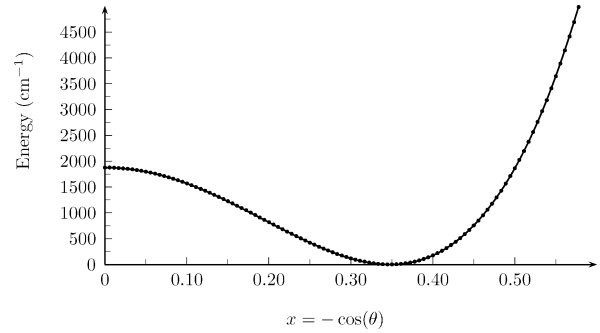

Figure 4. Lagrange interpolation (gray line) of the ab initio points (represented with dots) calculated with ρ frozen at the equilibrium value (see Figure 3). The values of the potential energy between the ab initio points are evaluated using a four-point Lagrange interpolation. See ref 20 for details.

solved by the hyperquantization algorithm to obtain the inversion energy levels. Figure 3 shows the potential energy of NH_3 as a function of the angle θ^g (see Figure 1). Dots represent 19 optimized ab initio points, obtained allowing for the NH bond length to relax. The same calculations carried out keeping fixed the NH distance at the equilibrium value (red line) show significant deviations with respect to the optimized ones. This means that the separability of the NH distances and the θ^g inversion coordinate gets lost. Figure 3 also shows that a profile obtained from calculations carried out with the hyperradius ρ at its equilibrium value, without optimization (blue line), appears to coincide with the optimized profile of the umbrella inversion path. This is an indication for us that in extensive calculations of ab initio points to be used as a grid for the hyperquantization method, the hyperradius can be frozen at its equilibrium value. The two symmetric minima (see also Table 3) are at $\theta^g = 67.7$ and 112.3°. The height of barrier ($\theta^g = 90°$ and $\theta = 90°$) between the two symmetric wells is 1867 cm^{-1}. These results are summarized in Table 3, where frequencies of the normal modes of vibration are also reported for the equilibrium and barrier configurations along with their assignment to hyperspherical coordinates. The mode resembling a low-amplitude umbrella inversion motion is the lower-frequency one with A1 symmetry and corresponds to our inversion coordinate θ. Due to the difference in frequency, this mode can be considered to be approximately separable with respect to the others, even farther from the equilibrium configuration. The θ coordinate tends to the limit of this mode for low amplitudes but enjoys separability also for a large-amplitude motion along the umbrella inversion path.

Figure 5 shows the moments of inertia, taken with respect to the x, y, and z axes of the NH_3 molecule (Figure 1), as a function of the hyperangle θ. The values are obtained by geometry optimization with respect to ρ. The data are compared with those calculated using the formulas of eqs 19, involving the coordinates θ and ρ. It is found that in the range of θ (see eq 14) that contains the two symmetric minima and the barrier of the potential profile (in the graph, where continuous curves and points coincide), the moments of inertia obtained from ab initio calculations and those calculated by the formulas are in very good agreement, meaning that θ and ρ (which has been frozen) reproduce with accuracy the inertia of the system. This further confirms that consideration of θ catches the essential of the inversion motion.

In Table 5, we show the inversion levels of the NH_3 molecule obtained by solving the eigenvalue problem for the operator of eq 21 by the hyperquantization method at fixed values of the hyperradius ρ. The inversion energy levels have been obtained

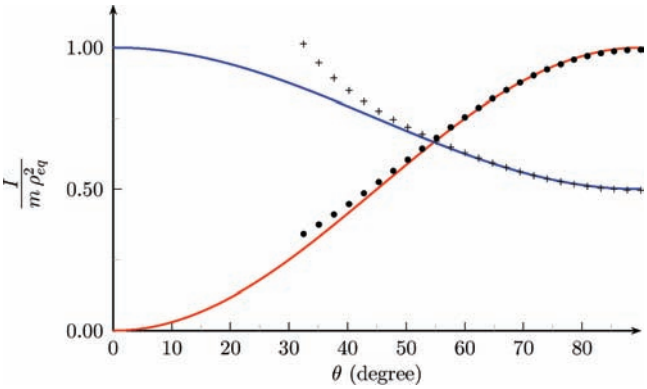

Figure 5. Moments of inertia with respect to the z axis (red line) and the x and y axes (blue line) of the NH_3 molecule (see Figure 1) as a function of the coordinate θ. The points represent the values of the moments of inertia calculated from ab initio geometries obtained at the CCSD(T) level with an aug-cc-pVQZ basis set and optimized with respect to the hyperradius ρ. The continuous lines represents the values obtained from eq 18 with ρ at its equilibrium value. The units are m ρ_{eq}^2.

using three different potential profiles calculated with the hyperradius ρ frozen at its equilibrium, barrier, and middle point between the minimum and the barrier values. Comparison is made with results available in the literature from both theory[7] and experiments[21] (sixth and seventh columns of the table).

As a test for our method, the same levels calculated using the potential energy surface developed by Halonen and co-workers[7] are reported and found to be in substantial agreement with those obtained from our potential profile, according to the fact that same level calculations have been carried out in the two cases.

While results are in general good agreement with those in the literature, major discrepancies are found in the range of energies similar to the barrier height where stronger coupling between the adiabatic eigenvalue curves is to be expected.

4.2. H_3O^+ Potential and Umbrella Inversion Levels. Table 4 shows the structural data obtained for the H_3O^+ molecule. This system also presents two symmetric minima at $\theta^g = 72.9$ and 107.1°. The barrier height at the planar configuration is 706.401 cm^{-1}, smaller than that for NH_3. Tunnel splitting is expected to be a relevant effect, and this is confirmed by the difference in energy between GS^+ and GS^- states shown in Table 6, reporting the inversion energy levels. As a consequence, only two states are found in the region of energies lower than the barrier height. The energy levels have been obtained using a potential energy surface developed by Halonen and co-workers.[8] It is seen that the energy level values calculated by the hyperquantization method are in good agreement with those obtained by a corresponding two-dimensional calculation.[8]

5. Discussion

The hyperquantization algorithm may seem demanding. For example, routinely, we used a grid of 3600 points that requires the diagonalization of a square matrix of order 3601. In the considered cases, the symmetry properties of the potential profile for the inversion coordinate θ (section 3) allow for a symmetry decomposition of the matrix into two submatrices of order 1801 (symmetric wave functions) and 1800 (antisymmetric wave functions). Our results for the umbrella levels, shown in Tables 5 and 6, are obtained by a one-dimensional calculation, while the values from literature required at least a two-dimensional approach for comparable accuracy. As can be seen, the agreement between the levels obtained here and those of the literature is quite good. In some cases and for particular applications, also to different molecules, a two-dimensional calculation may be necessary to guarantee sufficient or better accuracy.

The Lanczos diagonalization algorithm,[22] well suited for large sparse matrices, is of great help for our approach because of the tridiagonal form of the matrix **H**. This is true especially when the hyperquantization calculation scheme has to be repeated many times, for example, at several different values of the hyperradius ρ, which is the case of adiabatic eigenvalue calculation when the eigenvalues of the one-dimensional Hamiltonian operator used to calculate the inversion levels have to be obtained at many different values of ρ. The calculation scheme for adiabatic eigenvalue curves starts by setting ρ equal to a large value in the operator given in eq 20. Under this condition and the hypothesis of C_{3v} symmetry conservation, the potential energy function $V(\theta)$ tends to that of a square well, being approximately constant for $0 \ll \theta \ll \pi$, and steeply increases at the limits $\theta = 0$ and π. Each wave function can be approximated as a Legendre polynomial and, in the propagation of eigenvalues, these wave functions are used as a starting approximation for the solutions at the next value of ρ, smaller than the previous one. The scheme can then be repeated iteratively (see Figure 6) over the desired range of ρ, so that the propagation of the eigenvalues, either considering or neglecting the coupling terms, can then be efficiently performed.

Figure 6 shows the adiabatic eigenvalue curves, with respect to the r_{EB} parameter (see Figure 1), for NH_3 and H_3O^+, as obtained using, for the two molecules, the potential energy surfaces developed in refs 14 and 15. Note that r_{EB} is directly connected to the hyperradius ρ by eq 17. Symmetric and antisymmetric eigenvalues are plotted along with the valley bottoms (the minimum energy as a function of ρ) and ridges (the corresponding barrier heights) as a function of the r_{EB} distance for both symmetric and antisymmetric wave functions. Various isotopic variants have also been considered.

6. Final Remarks and Perspectives

In this work, we have shown that the umbrella inversion motion, typical of AB_3-type molecular systems, can be described with enough accuracy using Radau−Smith orthogonal vectors and parametrizing them by means of four-body hyperspherical coordinates, finding them particularly suited to describe the umbrella inversion motion, enforcing C_{3v} symmetry. We devised a one-dimensional model, freezing the remaining degrees of freedom to their equilibrium values, where the hyperangle θ catches all of the relavant aspects of the inversion dynamics. We have studied the two prototypical molecules NH_3 and H_3O^+, first demonstrating that the hyperspherical parametrization easily leads to a two-dimensional model involving the hyperangle θ and the hyperradius ρ. The model has been shown to be separable, the value of the hyperradius being conserved, when the molecule undergoes the inversion. The separability has been tested by ab initio calculations carried out by freezing ρ at different values, obtaining geometrical parameters for the molecules at their equilibrium and barrier configurations. The results show that the hyperradius can fairly be considered to be constant at its equilibrium value, and this ensures a good description of the inversion potential energy profile. From a one-dimensional eigenvalue problem, we have obtained accurate values of the inversion energy levels, comparable to those obtained by two-dimensional models so far adopted. The hyperquantization algorithm, so far used in quantum scattering

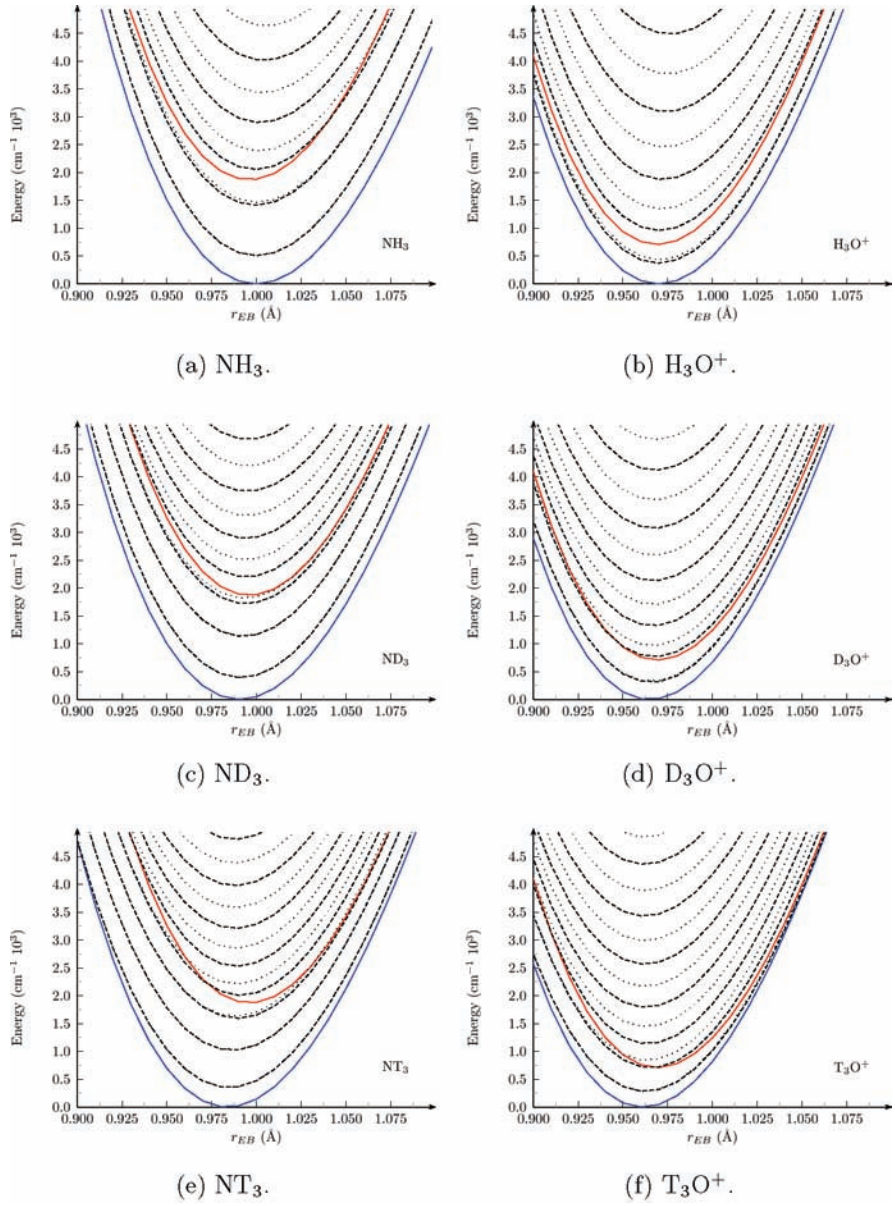

Figure 6. Adiabatic eigenvalues (calculated at fixed values of r_{EB}; see Figure 1)[14,15] for NH_3 and H_3O^+ systems obtained for the two-dimensional potential energy surfaces of refs 7 and 8. Blue line: valley bottoms; red line: ridges; dashed line: symmetric wave functions; dotted line: antisymmetric wave functions. The various panels show different isotopic variants.

calculations, has been applied to the solution of the eigenvalue problem for such an internal molecular dynamics study. The issue of the necessarily large discretization grid needed for this method, the possible source of computation time growth, has been circumvented by an efficient interpolation of reduced sets of ab initio points, a procedure which can be valid in general cases, not restricted to the application of the hyperquantization algorithm.

Results obtained in this work encourage us to recommend the angle θ for the description of the umbrella inversion in other systems. The one-dimensional approach permitted by the orthogonal coordinates and the performance of the hyperquantization algorithm should allow for a rapid exploration of the behavior of a variety of systems with C_{3v} symmetry. As a perspective, there is the generalization of our procedure to treat umbrella inversions in general. In particular, this is expected to be useful for quantum mechanical dynamics of molecular collisions.

The connection of four-body hyperspherical coordinates to normal modes of vibration of NH_3 and H_3O^+ has been also considered. This issue, being of general interest, will be the object of future work.

Acknowledgment. We acknowledge Andrea Beddoni for the contribution to the early stage of this research and for useful discussions. M.R. acknowledges Dimitri Mugnai of the Department of Mathematics of Perugia for useful discussions about mathematical details.

A. On the Centrosymmetric and Centroskew Matrices. (See also ref 16). The J is used to indicate square matrices with elements that obey to the relation $J_{i,j} = \delta_{n+1-i,j}$, where n represent the order of the matrices. For example, if $n = 3$

$$J = \begin{pmatrix} 0 & 0 & 1 \\ 0 & 1 & 0 \\ 1 & 0 & 0 \end{pmatrix} \tag{38}$$

A matrix M is centrosymmetric if

$$JMJ = M \tag{39}$$

It can be shown that for n even such a matrix can be written in terms of two matrices A and B of order $n/2$

$$M = \begin{pmatrix} A & BJ \\ JB & JAJ \end{pmatrix} \tag{40}$$

For odd n, one has

$$M = \begin{pmatrix} A & a & BJ \\ b & c & bJ \\ JB & Ja & JAJ \end{pmatrix} \tag{41}$$

where the matrices A and B have order $(n - 1)/2$, c is a scalar, and a and b are two vectors of order $(n - 1)/2$. For even n, one defines an orthogonal matrix K

$$K = \frac{2}{\sqrt{2}} \begin{pmatrix} I & -I \\ J & J \end{pmatrix} \tag{42}$$

where I is the identity matrix and the order of I and J matrices is $n/2$, which block-diagonalizes the M matrix

$$K^{-1}MK = \begin{pmatrix} A + B & 0 \\ 0 & A - B \end{pmatrix} \tag{43}$$

For odd n, the matrix K is

$$K = \frac{1}{\sqrt{2}} \begin{pmatrix} I & 0 & -I \\ 0 & \sqrt{2} & 0 \\ J & 0 & J \end{pmatrix} \tag{44}$$

where the order of the matrices I and J is $(n - 1)/2$ and

$$K^{-1}MK = \begin{pmatrix} A + B & a & 0 \\ b & c & 0 \\ 0 & 0 & A - B \end{pmatrix} \tag{45}$$

A matrix is "doubly symmetric" if A and B are symmetric with respect to both the principal and the secondary diagonals. If n is odd, the vector b is the transpose of a. Reference 16 treats also "skew-symmetric" matrices, which are equal to their transpose with a change in sign and "centro skew" if $M = -JMJ$.

References and Notes

(1) Aquilanti, V.; Maciel, G. S. *Origins Life Evol. Biosphere* **2006**, *32*, 435.

(2) Maciel, G. S.; Bitencourt, A. C. P.; Ragni, M.; Aquilanti, V. *Chem. Phys. Lett.* **2006**, *432*, 383390.

(3) Bitencourt, A. C. P.; Ragni, M.; Maciel, G. S.; Aquilanti, V.; Prudente, F. V. *J. Chem. Phys.* **2008**, *129*, 154316.

(4) Maciel, G. S.; Bitencourt, A. C. P.; Ragni, M.; Aquilanti, V. *Int. J. Quantum Chem.* **2007**, *107*, 26972707.

(5) Maciel, G. S.; Bitencourt, A. C. P.; Ragni, M.; Aquilanti, V. *J. Phys. Chem. A* **2007**, *111*, 12604.

(6) Aquilanti, V.; Ragni, M.; Bitencourt, A. C. P.; Maciel, G. S.; Prudente, F. V. *J. Phys. Chem. A* **2009**, *113*, 38043813.

(7) Pesonen, J.; Miani, A.; Halonen, L. *J. Chem. Phys.* **2001**, *115*, 1243.

(8) Miani, A.; Beddoni, A.; Pesonen, A.; Halonen, L. *Chem. Phys. Lett.* **2002**, *363*, 5256.

(9) Smith, F. T. *Phys. Rev. Lett.* **1980**, *45*, 1157.

(10) Ragni, M.; Bitencourt, A. C. P.; Aquilanti, V. *Int. J. Quantum Chem.* **2007**, *107*, 2870.

(11) Aquilanti, V.; Cavalli, S. *J. Chem. Soc., Faraday Trans.* **1997**, *93*, 801.

(12) Aquilanti, V.; Beddoni, A.; Cavalli, S.; Lombardi, A.; Littlejohn, R. *Mol. Phys.* **2000**, *98*, 1763. Beddoni, A. Ph.D. Thesis, University of Perugia, Italy, 2001.

(13) Anderson, R. W.; Aquilanti, V.; Cavalli, S.; Grossi, G. *J. Phys. Chem.* **1993**, *97*, 2443.

(14) Aquilanti, V.; Cavalli, S.; De Fazio, D. *J. Chem. Phys.* **1998**, *109*, 3792.

(15) Aquilanti, V.; Cavalli, S.; Volpi, A. *Adv. Quantum Chem.* **2001**, *39*, 103.

(16) Collar, A. R. *Q. J. Mech. Appl. Math.* **1962**, *15*, 265.

(17) Barreto, P. R. P.; Vilela, A. F. A.; Lombardi, A.; Maciel, G.; Palazzetti, F.; Aquilanti, V. *J. Phys. Chem. A* **2007**, *111*, 12754.

(18) Maciel, G. A.; Barreto, P. R. P.; Lombardi, A.; Palazzetti, F.; Aquilanti, V. *J. Chem. Phys.* **2008**, *129*, 164302.

(19) Frisch, M. J.; Trucks, G. W.; Schlegel, H. B.; Scuseria, G. E.; Robb, M. A.; Cheeseman, J. R.; Montgomery, J. A., Jr.; Vreven, T.; Kudin, K. N.; Burant, J. C.; Millam, J. M.; Iyengar, S. S.; Tomasi, J.; Barone, V.; Mennucci, B.; Cossi, M.; Scalmani, G.; Rega, N.; Petersson, G. A.; Nakatsuji, H.; Hada, M.; Ehara, M.; Toyota, K.; Fukuda, R.; Hasegawa, J.; Ishida, M.; Nakajima, T.; Honda, Y.; Kitao, O.; Nakai, H.; Klene, M.; Li, X.; Knox, J. E.; Hratchian, H. P.; Cross, J. B.; Bakken, V.; Adamo, C.; Jaramillo, J.; Gomperts, R.; Stratmann, R. E.; Yazyev, O.; Austin, A. J.; Cammi, R.; Pomelli, C.; Ochterski, J. W.; Ayala, P. Y.; Morokuma, K.; Voth, G. A.; Salvador, P.; Dannenberg, J. J.; Zakrzewski, V. G.; Dapprich, S.; Daniels, A. D.; Strain, M. C.; Farkas, O.; Malick, D. K.; Rabuck, A. D.; Raghavachari, K.; Foresman, J. B.; Ortiz, J. V.; Cui, Q.; Baboul, A. G.; Clifford, S.; Cioslowski, J.; Stefanov, B. B.; Liu, G.; Liashenko, A.; Piskorz, P.; Komaromi, I.; Martin, R. L.; Fox, D. J.; Keith, T.; Al-Laham, M. A.; Peng, C. Y.; Nanayakkara, A.; Challacombe, M.; Gill, P. M. W.; Johnson, B.; Chen, W.; Wong, M. W.; Gonzalez, C.; Pople, J. A. *Gaussian 03*, revision D.01; Gaussian, Inc.: Wallingford, CT, 2004.

(20) Abramowitz M. Stegun A. *Handbook of Mathematical Functions*; eqs.25.2.9 and 25.2.13, Dover Publications: U.K., 1965.

(21) Špirko, S V. *J. Mol. Spectrosc* **1983**, *101*, 30.

(22) Lanczos algorithm; http://en.wikipedia.org/wiki/Lanczos algorithm, 2009.

(23) Verhoeve, P.; Versluis, M.; Termeulen, J. J.; Meerts, W. L.; Dymanus, A. *Chem. Phys. Lett.* **1989**, *161*, 195.

(24) Petek, H.; Liu, D. J.; Oka, T.; Sears, T. J. *J. Chem. Phys.* **1986**, *84*, 1312.

(25) Davies, P. B.; Johnson, S. A.; Hamilton, P. A.; Sears, T. J. *Chem. Phys.* **1989**, *108*, 335.

(26) (a) Chase, M. W. *J. Phys. Chem. Ref. Data* **1998**, Monograph 9. (b) Shimamouchi, T. *J. Phys. Chem. Ref. Data* **1977**, *6*, 993.

(27) Špirko, S V.; Kraemer, W. P. *J. Mol. Spectrosc.* **1989**, *133*, 331.

(28) Rajamäki, T.; Miani, A.; Halonen, L. *J. Chem. Phys.* **2003**, *118*, 10929.

(29) Tang, J.; Oka, T. *J. Mol. Spectrosc.* **1999**, *196*, 120.

JP906415M